Eur. Phys. J. D (2021) 75:124
https://doi.org/10.1140/s10053-021-00112-9

THE EUROPEAN PHYSICAL JOURNAL D

Regular Article - Clusters and Nanostructures

Submersion of rubidium clusters in helium nanodroplets

Arne Schiller[1,a], Paul Martini[1], Elias Emile Jabbour Al Maalouf[2], and Paul Scheier[1]

[1] Institut für Ionenphysik und Angewandte Physik, Universität Innsbruck, Technikerstr. 25, 6020 Innsbruck, Austria
[2] Faculté des Sciences IV, Université Libanaise, Haouch El-Omara, Zahlé, Lebanon

Received 3 November 2020 / Accepted 9 December 2020 / Published online 12 April 2021

Abstract. Alkali atoms and small clusters are known to reside on the surface of a helium droplet rather than its inside as most other dopant species. A theoretical investigation suggested that alkali clusters (Li–Rb) exceeding a certain critical size can become submerged in the droplet, which was experimentally confirmed for sodium and potassium. Here, we report an analogous experimental study of rubidium cluster submersion by means of electron impact mass spectrometry. We recorded size distributions of Rb cluster ions at various electron energies between 8 and 160 eV. Our data suggest that Rb clusters attached to helium droplets undergo a gradual submersion transition similar to potassium, ultimately leading to the full submersion of clusters larger than ∼ 100 Rb atoms. Our findings are consistent with previous theoretical and experimental studies.

1 Introduction

Superfluid helium nanodroplets (HNDs) possess the unique ability to pick up virtually any gas-phase atoms or molecules (called dopants) they collide with [1–3] and allow them to coagulate or react [4–11] at their characteristic temperature of 0.37 K [12]. This has been widely exploited, e.g., for spectroscopy [13–18], studying chemical reactions [19–24] or synthesizing nanomaterials [25–32]. Whereas for most dopant atoms and molecules, a location in the interior of the HND is energetically favorable [33–38], alkali metal atoms are a prominent exception from this rule [39–42]. They are found to reside in surface dimples due to a short-range Pauli repulsion between their s valence electrons and surrounding helium atoms counteracting the van der Waals attractive force(s) [43,44]. While this holds true for small alkali clusters, Stark and Kresin used a classical model to predict that with increasing cluster size, the attractive forces grow faster than the repulsive ones, enabling sufficiently large alkali clusters to become submerged in the HND [45]. Stark and Kresin calculated the critical sizes n_c as 23, 21, 78, 131 and 625 for submersion of Ak_n where Ak = Li, Na, K, Rb and Cs, respectively. The last two values are interpreted as submersion of Rb_n with $n > 100$ and a lack of submersion into the HND for cesium. Lithium does not form large enough neutral clusters on the surface of HNDs that could eventually submerge into the droplets. Their binding energy to the HNDs is so low that the conversion from small high-spin state clusters to their ground state configuration will boil them off. The largest Li_n^+ cluster that we have observed so far is the trimer. Following a proposition of Stark and Kresin to experimentally verify their predictions [45], An der Lan et al. conducted two studies utilizing HNDs doped with sodium [46] and potassium [47] by exploiting the electron ionization (EI) and electron excitation (EA) characteristics of HNDs. Whereas incident electrons with energies between 19.8 and 24.6 eV cannot directly ionize He atoms, they may produce metastable excited He* or He_2*, which can ionize almost any dopant atom or molecule by transfer of its excitation energy upon collision. Unlike He^+ or He_2^+ and most dopants, which migrate toward the interior of the HND, He* or He_2* will—like alkali atoms and small alkali clusters—locate at or near the droplet surface for the same reasons [48–50]. By monitoring the ion yield of alkali clusters as a function of cluster size and electron energy, the authors were able to identify a transition in the ionization characteristics consistent with a submersion into the HND. The experimentally determined submersion sizes $n_{c,\mathrm{exp}} = 21$ and ∼ 80 for Na_n and K_n, respectively, are in remarkably good agreement with the theoretical predictions. However, whereas the surface → interior transition of Na_n is sharp, the submersion of K_n appears to be more gradual. For the next larger alkali metal, rubidium, the transition is expected to be even more diffuse [47]. Here, we apply the concept used by An der Lan and co-workers to rubidium clusters in an effort to experimentally determine their critical submersion size.

Supplementary information The online version of this article (https://doi.org/10.1140/s10053-021-00112-9) contains supplementary information, which is available to authorized users.

[a] e-mail: arne.schiller@uibk.ac.at (corresponding author)

2 Experimental

The experimental apparatus is described in detail elsewhere [46,51]. Briefly, HNDs are produced in a supersonic expansion of ultra-pure helium (He 6.0, 99.9999% purity) at a temperature of 9.4 K and stagnation pressure of 22 bar, yielding an average size of $\sim 5 \times 10^5$ He atoms per droplet [51]. The HND beam passes a skimmer, followed by two differentially pumped pickup chambers in one of which Rb vapor (Sigma-Aldrich, 99.6% purity) is added from a resistively heated oven kept at 80°C. While we cannot measure the doping pressure right above the heated oven, we can estimate it to lie between the Rb partial pressure in the doping chamber measured at 2.5×10^{-6} mbar and, probably closer to, the vapor pressure of Rb at 80°C, which is $\sim 7.5 \times 10^{-5}$ mbar [52]. The doped droplets then enter a differentially pumped chamber where they are subject to an incident electron beam (energy spread > 1 eV). Ions ejected from the HNDs upon EI/EA [1] are analyzed in a high-resolution time-of-flight mass spectrometer (ToF-MS) which typically reaches a resolving power of up to $m/\Delta m \approx 5000$ [53], but is limited to $m/\Delta m \approx 2000$ in this study due to the large mass range extending to over 17000 amu or 200 Rb atoms. Several mass spectra with acquisition times between 30 min and 20 h were recorded at electron energies between 21.6 and 160 eV, along with an electron energy scan between 8 and 38 eV. Resulting cluster distributions shown in this paper were extracted from the recorded mass spectra with the IsotopeFit analysis software where possible [54].

3 Results/discussion

3.1 Energy scan

We will start our analysis with the results of the recorded electron energy scan. The relative yield of selected ions as a function of electron energy between 8 and 38 eV is shown in Fig. 1. The notable features can be explained by considering that the energy range can be divided into three different regimes:

1. At electron energies below 19.8 eV, no He excitation is possible. Negligible ion yields of smaller Rb ions can be observed, most likely due to direct EI of surface-bound Rb clusters or the finite energy spread of the incident electron beam.
2. Between 19.8 and 24.6 eV (shaded area in Fig. 1), several resonances for electronic excitation of He exist. Metastable excited He* or He_2* are heliophobic and will migrate toward the droplet surface. They may ionize dopants located there or near it via Penning ionization, explaining the considerable yield of smaller Rb_n^+ in this region. Subthreshold ionization of He is also possible via a Penning process where two electronically excited He atoms are required [55].
3. Electrons with an energy in excess of 24.6 eV may directly ionize He, and while excitations are still possible, they become increasingly inefficient relative to the direct ionization of He [56,57]. A nascent He^+ will migrate toward the droplet center by resonant charge hopping between neighboring He atoms [58–60]. A dopant (cluster) located in the HND interior may be ionized directly upon encountering He^+ or He_2^+, the latter being typically formed after some $\sim$ 10 hops [59]. In this regime, a strong increase in the relative yield of larger Rb_n^+ is observed.

The ion yield curves shown in Fig. 1 already contain strong evidence for an exterior → interior transition of Rb clusters. Small Rb molecules and clusters show a distinct local maximum in ion yield around 23 eV, indicating efficient Penning ionization via He* and He_2* and thus an exterior location. This feature gradually weakens for larger clusters, whereas the increase in relative ion yield beyond $\sim$ 25 eV gets progressively stronger for larger Rb_n^+. The shapes of the ion yield curves of larger Rb_n^+ (e.g., Rb_9^+ in Fig. 1) compare favorably to those of heliophilic species recorded in separate experiments at the same apparatus (Fig. S1) and are thus consistent with an interior location of larger Rb clusters. We carefully checked for alternative explanations that could arise due to the fact that the enhanced pickup cross section of larger droplets favors the formation of larger Rb clusters. Since HNDs have a size distribution

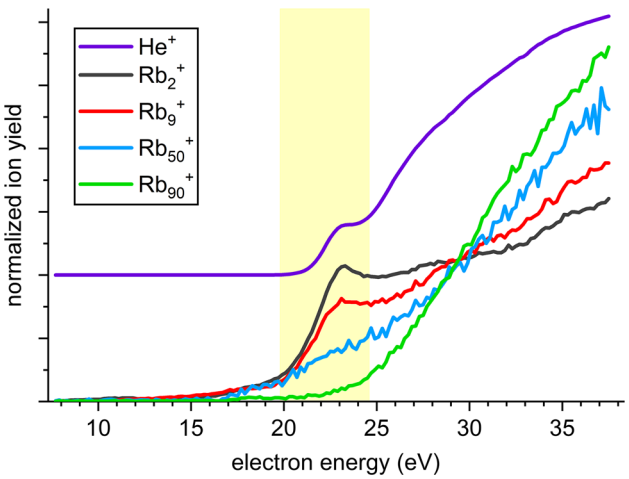

Fig. 1 Normalized yield of selected cluster ions as a function of electron energy. The He^+ curve is offset for better visibility. This curve is expected to increase in a linear fashion above 25 eV, and its flattening above 27 eV is caused by detector saturation. In the shaded region between 19.8 and 24.6 eV, He^+ as well as the two smaller Rb cluster ions display a prominent hump caused by a Penning process. While this feature is gradually disappearing toward larger Rb clusters, an increasingly steep gradient in relative ionization efficiency toward higher electron energies is noticeable with increasing cluster size

of their own, it is conceivable that the observed change of ionization characteristics for larger Rb_n^+ is indicative of the HND size rather than the dopant location. We were, however, unable to find any evidence for a strong influence of the droplet size on our measurements (cf. Fig. S1). The apparent transition from an exterior to an interior location appears to proceed gradually with no abrupt changes immediately noticeable from the ion yield curves, so it is difficult to identify a critical size at which a Rb cluster is fully submerged in the HND. An der Lan and co-workers noticed that the transition in K clusters [47] was much more diffuse than for Na [46], suggesting it would be even more diffuse for Rb [47], in good agreement with our observation. In their study of potassium clusters, An der Lan et al. fitted the ion efficiency curves of K_n^+ clusters via a superposition of the ion efficiency curves of K_2^+ and K_{90}^+. The contribution from K_2^+ exhibits a resonance at about 22 eV and is remarkably similar to the cross section of He* formation and thus indicating Penning ionization of small neutral potassium clusters contribution to the ion yield of K_2^+. In contrast, the contribution from K_{90}^+ is sharply increasing at electron energies higher than 25 eV, which suggests that large neutral potassium clusters ionized via charge transfer from He^+ or He_2^+ inside the HND are predominantly forming K_{90}^+. The relative contributions of K_2^+ and K_{90}^+ that reproduced the ion efficiency curves of a given potassium cluster ion were then used as a measure of the degree of cluster submersion. Unfortunately, this approach is not feasible for our data since the ion yields are fairly low, especially for large clusters, making a fitting of the ion yield curves difficult and prone to large statistical errors. We will therefore attempt a different, but perhaps superior method for the determination of the critical submersion size by using mass spectra recorded at a fixed electron energy, which feature a much better signal-to-noise ratio.

3.2 Mass spectra

Before we attempt to identify the critical size for submersion of Rb clusters in HNDs, we shall give a brief overview over some of the recorded mass spectra. In Fig. 2, we show an excerpt of a mass spectrum of Rb-doped HNDs recorded at an electron energy of 21.6 eV extending to about 4000 amu or 45 Rb atoms. The notable features in this region were qualitatively very similar in all mass spectra. We find several local anomalies in the cluster size distribution, such as strong odd–even oscillations, most notably up to $n = 16$, as well as abrupt drops in the abundance of Rb_n^+ after so-called magic number clusters [61–65], e.g., after $n = 5$, 9, 21 and 41. These local anomalies can be understood by considering that both excitation and charge transfer from He to the dopant are highly exoergic processes. The emanating cluster ion is generally formed in a highly excited, "hot" state, leading to fragmentation as a possible way of dissipating excess energy. This process leads to a depletion of less stable cluster ions and a corresponding enrichment of particularly stable sizes

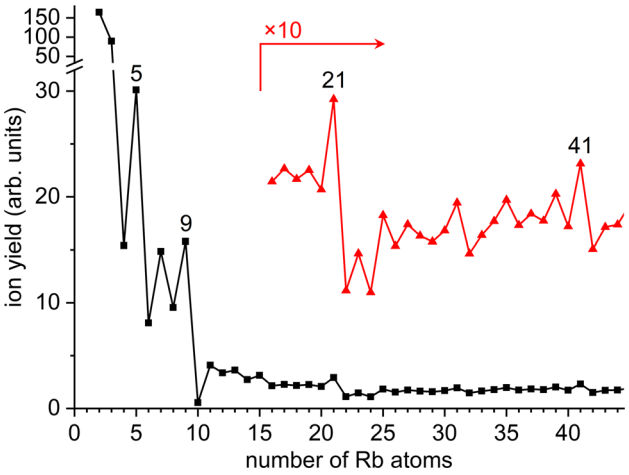

Fig. 2 Lower-mass portion of a cluster size distribution extracted from a mass spectrum of Rb clusters grown in large HNDs ($N_{He} \sim 5 \times 10^5$), recorded at an electron energy of 21.6 eV. Prominent local anomalies corresponding to cluster sizes of higher stabilities and/or electronic shell closures are marked in the mass spectrum. The notable features in this mass range are equally observed in mass spectra recorded at higher electron energies of 40, 70 and 160 eV

in the mass spectra. Whereas the overall abundance distribution is mostly governed by the pickup statistics (i.e., the size distribution of neutral dopant clusters), variations in this envelope directly reflect the relative stability of the corresponding cluster ions. The observed odd–even oscillations and magic numbers are equally found for all other Ak_n^+ (Ak = Li−Cs) [62,66–70] and can be explained in terms of an electronic shell model where the cluster ion is described as an $(n-1)$ electron system. Odd-numbered Ak_n^+ and especially magic number clusters are considered particularly stable due to an even number of electrons (i.e., only paired electrons), whereas the observed magic numbers additionally correspond to the complete filling of electronic shells (similar to rare gas atoms) [71].

Figure 3a shows a comparison of two cluster distributions extracted from the higher-mass portion (∼ 3300–17000 amu or 40–200 Rb atoms) of mass spectra recorded at electron energies of 21.6 eV and 40 eV, respectively. Apart from the electron energy, all other experimental settings (i.e., HND source settings, Rb oven temperature, ion optics and ToF-MS settings) were identical. The cluster size distributions are fairly similar until ∼ 60 Rb atoms (see discussion about Fig. 2), but markedly different toward higher numbers of Rb atoms. The cluster ion yield at 21.6 eV first increases toward 60 Rb atoms but drops off sharply afterward and levels out at negligible values around ∼ 95 Rb atoms. It should be noted that a distinct drop after $n = 93$, which is also apparent in the 40 eV distribution, coincides with an electronic shell closure, indicating a magic number cluster. In contrast, the ion yield recorded at 40 eV continues to rise and displays a broad maximum around ∼ 95 Rb atoms before grad-

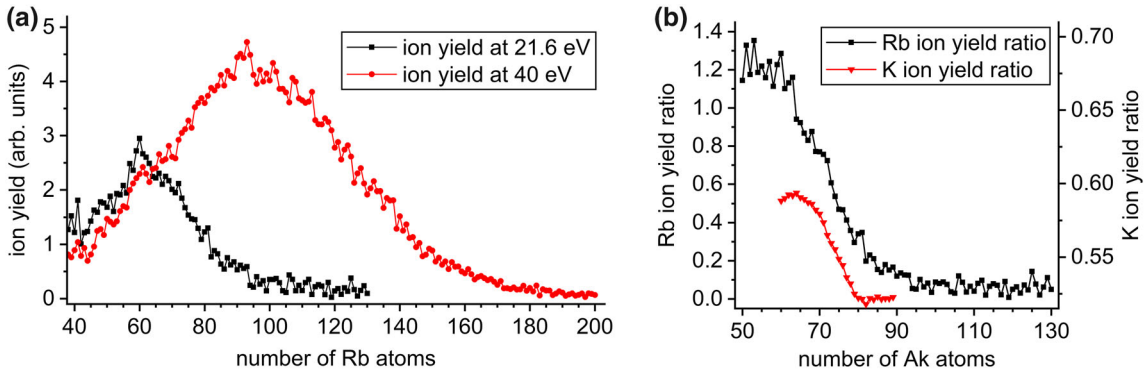

Fig. 3 **a** Higher-mass portion of cluster size distributions extracted from mass spectra of Rb clusters grown in large HNDs ($\sim 5 \times 10^5$), recorded at electron energies of 21.6 and 40 eV, respectively. The gradual submersion of Rb clusters into the HND is evident from the decrease in ion yield between 60 and 100 atoms in the 21.6 eV mass spectrum. The 40 eV mass spectrum is governed by Poissonian pickup statistics, possibly limited by a decrease in detection efficiency toward larger masses. **b** Ratio of ion yields recorded at 21.6 and 40 eV for Rb. A gradual decline of ion yield ratio corresponding to a submersion into the HND is noticeable starting around 50 Rb atoms. Rubidium clusters larger than $\sim$ 100 atoms are assumed to be fully submerged. Also shown is a re-evaluation of K data by An der Lan et al. [47] at electron energies of 21.5 and 27.5 eV, suggesting a similar submersion transition around 80 K atoms

ually declining with the last discernible cluster ion signals at $\sim$ 200 Rb atoms. The 40 eV mass spectrum more closely resembles a log-normal shape, which is expected for the size distribution of neutral clusters due to Poissonian pickup statistics [72] into differently sized HNDs that follow a log-normal size distribution as well [73]. It is possible that the cluster size distribution actually extends further but is discriminated due to a declining detector efficiency and/or ion transmission in the high-mass region.

3.3 Critical submersion size

As previously discussed, at an electron energy of 21.6 eV, dopant ionization occurs primarily at or near the HND surface via Penning ionization by He* or He_2* while at 40 eV, dopant ionization primarily occurs in the droplet interior via charge transfer from He^+ and He_2^+. While cluster ions larger than $\sim$ 100 Rb atoms are notably absent in the 21.6 eV mass spectrum, they are abundant in the 40 eV spectrum. Since all experimental parameters except the electron ionization energy are equal, neutral clusters of at least the size indicated by the 40 eV spectrum must also be present in the 21.6 eV experiment but fail to show up as ions. This fact is taken as an indication for the full submersion of Rb clusters around $\sim$ 95 Rb atoms. Similar to the energy scan curves, it appears difficult to make out a precise critical submersion size $n_{c,\mathrm{exp}}$ from the presented mass spectra. As previously discussed, this is not surprising, as a fairly diffuse transition is expected for rubidium [47]. In an attempt to more precisely determine $n_{c,\mathrm{exp}}$, we calculated the ratio of ion yields of the previously discussed mass spectra at 21.6 and 40 eV for every cluster ion. The results, shown in Fig. 3b, are similar if mass spectra at different low and high energies are used for analysis. Higher ion yield ratios indicate a relatively more efficient Penning versus charge transfer ionization, pointing toward a surface location of the corresponding neutral cluster, whereas lower values suggest the corresponding neutral cluster is submerged in the HND to a higher degree. Similar to the mass spectra, we see a sharp decline starting around 60 Rb atoms, which becomes less steep around 80 Rb atoms and finally levels out around 100 Rb atoms.

In order to test our method, we re-evaluated the potassium data by An der Lan et al. in the critical size range, shown alongside our Rb data in Fig 3b. We find a pronounced transition around $n_{c,\mathrm{exp}} \approx 80$, in good agreement with the evaluation of An der Lan et al. [47] and the prediction of Stark and Kresin [45]. Since there is good agreement with the above-mentioned studies and the transition found with our method appears much sharper, we conclude that this method of evaluation should be reasonable, if not better than the fitting method. For Rb, however, we still observe a fairly smooth transition, making it difficult to assign a critical submersion size. Before we attempt to do so, we will discuss two effects that might skew our assignment toward smaller Rb cluster sizes. As Stark and Kresin [45] as well as An der Lan et al. [47] pointed out, there is a more delicate balance between repulsive and attractive forces in the transition region for clusters of heavier alkali species, leading to an increasingly gradual submersion. The shrinking of the HND due to evaporation of He upon pickup and coagulation of dopant Rb atoms might play an additional role and exaggerate this effect. We can estimate that for the assembly of a Rb_{100} cluster, $\sim$ 50 meV kinetic and $\sim$ 0.65 eV binding energy [74] per Rb atom or 70 eV in total have to be dissipated by the HND. Assuming an energy release of 0.6 meV upon evaporation of one He atom [75], this would shrink the HND by $\sim 10^5$ He atoms. This is considerable compared to the average size of $\sim 5 \times 10^5$ He atoms per HND, meaning that the lower portion of the HND size distribution would get largely evapo-

rated. Consequently, a large Rb cluster grown in a small HND would be located closer to the surface and could thus be ionized efficiently at 21.6 eV, either directly or by a Penning process, despite being large enough to be fully submerged. On the other hand, large Rb clusters are less likely to be formed in small droplets due to the smaller geometric cross section for the pickup of Rb atoms. Taking into account that such smaller droplets typically represent less than a few percent of the droplet size distribution, we conclude that the discussed shrinking of droplets should not significantly affect our assignment.

A second effect could arise due to a common problem with mass spectrometry of doped HNDs in that we can only measure the distribution of cluster ions *after* the ionization process. As previously discussed, He-mediated ionization is generally highly exoergic and might induce fragmentation of the emanating cluster ions, which would manifest in a mass spectrum shifted toward smaller cluster sizes. However, larger clusters are generally more robust against fragmentation since excess energy can be stored in the larger number of internal degrees of freedom, while the emanating cluster ion is cooled via evaporation of He atoms from the droplet. This is also evident from the mass spectra, which are highly structured at smaller cluster sizes, especially below $n = 15$, whereas at higher masses, the spectra show a much smoother cluster size distribution. This indicates that while smaller cluster ions are probably subject to intense fragmentation, it is diminished for larger clusters. Consequently, it is likely that the size distribution of larger cluster ions closely resembles that of neutral clusters, leading us to conclude that fragmentation should not have a big influence on our assignment.

In summary, we consider both effects discussed above to be negligible and thus experimentally assign the critical size for submersion of Rb clusters into HNDs at ~ 100 atoms. Whereas Stark and Kresin's calculation yields 131 atoms [45], they interpret this result carefully and rather give an estimate of > 100 atoms as a critical submersion size, in decent agreement with our results. It appears that while the simple model works remarkably well for the smaller alkali species Na and K, its predictions become less accurate for the larger Rb, and likely Cs as well, for which a failure of submersion is predicted. Considering, however, that the model appears to overestimate the critical submersion size of Rb, it would be interesting to see whether revised theoretical work arrives at the same conclusion for Cs. This would also help to determine whether an experimental observation of Cs cluster submersion into HNDs is feasible. With our present setup, this is highly questionable, even if the critical submersion size was considerably lower than calculated by Stark and Kresin [45].

4 Conclusion

We performed an experimental study based on the studies of An der Lan et al. [46,47] aiming to determine the critical size of rubidium cluster for submersion in HNDs. Rb clusters with over 200 atoms were observed in EI mass spectra of Rb-doped HNDs. The cluster size distribution showed well-known features of alkali clusters such as odd–even oscillations and magic numbers such as $n = 9$, 21 and 41, which correspond to electronic shell closures. We then compared the ion yield for different cluster sizes obtained from mass spectra recorded at electron energies of 21.6 and 40 eV as a measure of submersion. We observed a rather gradual transition from an exterior to an interior location of Rb clusters as a function of cluster size. Our analysis suggests full submersion of Rb clusters larger than ~ 100 atoms, in good agreement with a theoretical model by Stark and Kresin [45]. Future theoretical and experimental work is encouraged to determine whether such a transition is also feasible for cesium clusters.

Acknowledgements This work was supported by the Austrian Science Fund FWF, Project number P31149.

Author contributions

AS and PM performed the experiment. AS and EEJM evaluated the data. AS and PS prepared the manuscript. PS supervised the study. All authors have read and approved the manuscript.

Funding Open access funding provided by University of Innsbruck and Medical University of Innsbruck.

Data Availability Statement This manuscript has no associated data or the data will not be deposited. [Authors' comment: The data supporting the findings of this study are available from the authors upon request.]

References

1. A. Mauracher et al., Cold Physics and Chemistry: Collisions, Ionization and Reactions inside Helium Nanodroplets Close to Zero K. Phys. Rep. **751**, 1–90 (2018). https://doi.org/10.1016/j.physrep.2018.05.001
2. J.P. Toennies, A.F. Vilesov, Superfluid Helium Droplets: A Uniquely Cold Nanomatrix for Molecules and Molecular Complexes. Angew. Chem. Int. Edit. **43**, 2622–2648 (2004). https://doi.org/10.1002/anie.200300611
3. A. Scheidemann et al., Capture of Neon Atoms by ^{4}He Clusters. Phys. Rev. Lett. **64**, 1899–1902 (1990). https://doi.org/10.1103/PhysRevLett.64.1899
4. E. Lugovoj et al., Manipulating and enhancing chemical reactions in helium droplets. J. Chem. Phys. **112**, 8217–8220 (2000). https://doi.org/10.1063/1.481426
5. M. Farnik, J.P. Toennies, Ion-molecule reactions in ^{4}He droplets: Flying nano-cryo-reactors. J. Chem. Phys. **122**, 11 (2005). https://doi.org/10.1063/1.1815272
6. A. Kaiser et al., Adsorption of hydrogen on neutral and charged fullerene: Experiment and theory. J. Chem. Phys. **138**, 074311–13 (2013). https://doi.org/10.1063/1.4790403
7. S. Denifl et al., Ion-Molecule Reactions in Helium Nanodroplets Doped with C_{60} and Water Clusters. Angew. Chem.-Int. Edit. **48**, 8940–8943 (2009). https://doi.org/10.1002/anie.200904381
8. S. Müller et al., Cold Reactions of Alkali-Metal and Water Clusters inside Helium Nanodroplets. Phys. Rev. Lett. **102**, 183401 (2009). https://doi.org/10.1103/PhysRevLett.102.183401
9. S.A. Krasnokutski, F. Huisken, Oxidative Reactions of Silicon Atoms and Clusters at Ultra low Temperature in Helium Droplets. J. Phys. Chem. A **114**, 13045–13049 (2010). https://doi.org/10.1021/jp110323n
10. S.A. Krasnokutski, F. Huisken, Ultra-Low-Temperature Reactions of Mg Atoms with O_2 Molecules in Helium Droplets. J. Phys. Chem. A **114**, 7292–7300 (2010). https://doi.org/10.1021/jp103947z
11. S.A. Krasnokutski, F. Huisken, Reactivity of Iron Atoms at Low Temperature. J. Phys. Chem. A **118**, 2612–2617 (2014). https://doi.org/10.1021/jp5007704
12. M. Hartmann et al., Rotationally Resolved Spectroscopy of SF_6 in Liquid Helium Clusters: A Molecular Probe of Cluster Temperature. Phys. Rev. Lett. **75**, 1566–1569 (1995). https://doi.org/10.1103/PhysRevLett.75.1566
13. D. Verma et al., Infrared spectroscopy in superfluid helium droplets. Adv. Phys.-X **4**, 32 (2019). https://doi.org/10.1080/23746149.2018.1553569
14. M.Y. Choi et al., Infrared spectroscopy of helium nanodroplets: novel methods for physics and chemistry. Int. Rev. Phys. Chem. **25**, 15–75 (2006). https://doi.org/10.1080/01442350600625092
15. C. Callegari et al., Helium nanodroplet isolation rovibrational spectroscopy: Methods and recent results. J. Chem. Phys. **115**, 10090–10110 (2001). https://doi.org/10.1063/1.1418746
16. C. Callegari, W.E. Ernst, *Helium Droplets as Nanocryostats for Molecular Spectroscopy–from the Vacuum Ultraviolet to the Microwave Regime* (John Wiley & Sons Ltd, In Handbook of High-Resolution Spectroscopy, 2011)
17. S. Grebenev et al., Superfluidity within a small helium-4 cluster: The microscopic Andronikashvili experiment. Science **279**, 2083–2086 (1998). https://doi.org/10.1126/science.279.5359.2083
18. J.P. Toennies, A.F. Vilesov, Spectroscopy of atoms and molecules in liquid helium. Annu. Rev. Phys. Chem. **49**, 1–41 (1998). https://doi.org/10.1146/annurev.physchem.49.1.1
19. S.A. Krasnokutski, F. Huisken, Low-Temperature Chemistry in Helium Droplets: Reactions of Aluminum Atoms with O_2 and H_2 O. J. Phys. Chem. A **115**, 7120–7126 (2011). https://doi.org/10.1021/jp112423v
20. S.A. Krasnokutski et al., Ultra-Low-Temperature Reactions of Carbon Atoms with Hydrogen Molecules. Astrophys. J. Lett. **818**, L31 (2016). https://doi.org/10.3847/2041-8205/818/2/L31
21. M. Daxner et al., Electron-Driven Self-Assembly of Salt Nanocrystals in Liquid Helium. Angew. Chem. Int. Ed. **53**, 13528–13531 (2014). https://doi.org/10.1002/anie.201409465
22. M. Renzler et al., Communication: Dopant-induced solvation of alkalis in liquid helium nanodroplets. J. Chem. Phys. **145**, 4 (2016). https://doi.org/10.1063/1.4967405
23. M. Harnisch et al., Adsorption of sodium and cesium on aggregates of C_{60}. Eur. Phys. J. D **70**, 8 (2016). https://doi.org/10.1140/epjd/e2016-70438-4
24. M. Renzler et al., Positively and Negatively Charged Cesium and $(C_{60})_mCs_n$ Cluster Ions. J. Phys. Chem. C **121**, 10817–10823 (2017). https://doi.org/10.1021/acs.jpcc.6b11928
25. L.F. Gomez et al., Traces of Vortices in Superfluid Helium Droplets. Phys. Rev. Lett. **108**, 155302 (2012). https://doi.org/10.1103/PhysRevLett.108.155302
26. S.F. Yang, A.M. Ellis, Helium droplets: a chemistry perspective. Chem. Soc. Rev. **42**, 472–484 (2013). https://doi.org/10.1039/c2cs35277j
27. A. Boatwright et al., Helium droplets: a new route to nanoparticles. Faraday Discuss. **162**, 113–124 (2013). https://doi.org/10.1039/C2FD20136D
28. P. Thaler et al., Synthesis of nanoparticles in helium droplets-A characterization comparing mass-spectra and electron microscopy data. J. Chem. Phys. **143**, 10 (2015). https://doi.org/10.1063/1.4932182
29. G. Haberfehlner et al., Formation of bimetallic clusters in superfluid helium nanodroplets analysed by atomic resolution electron tomography. Nat. Commun. **6**, 8779 (2015). https://doi.org/10.1038/ncomms9779
30. M. Schnedlitz et al., Effects of the Core Location on the Structural Stability of Ni-Au Core-Shell Nanoparticles. J. Phys. Chem. C **123**, 20037–20043 (2019). https://doi.org/10.1021/acs.jpcc.9b05765
31. A. Schiffmann et al., Helium droplet assisted synthesis of plasmonic Ag@ZnO core@shell nanoparticles. Nano Res. **13**, 2979–2986 (2020). https://doi.org/10.1007/s12274-020-2961-z
32. M. Schnedlitz et al., Thermally Induced Diffusion and Restructuring of Iron Triade (Fe Co, Ni) Nanoparticles Passivated by Several Layers of Gold. J. Phys. Chem. C **124**, 16680–16688 (2020). https://doi.org/10.1021/acs.jpcc.0c04561
33. D. Buchta et al., Charge Transfer and Penning Ionization of Dopants in or on Helium Nanodroplets Exposed

to EUV Radiation. J. Phys. Chem. A **117**, 4394–4403 (2013). https://doi.org/10.1021/jp401424w
34. J. Poms et al., Helium nanodroplets doped with xenon and rubidium atoms: a case study of van der Waals interactions between heliophilic and heliophobic dopants. Phys. Chem. Chem. Phys. **14**, 15158–15165 (2012). https://doi.org/10.1039/C2CP42333B
35. G.E. Douberly et al., $(HCN)_mM_n$ (M = K, Ca, Sr): Vibrational Excitation Induced Solvation and Desolvation of Dopants in and on Helium Nanodroplets. J. Phys. Chem. A **114**, 3391–3402 (2010). https://doi.org/10.1021/jp908834m
36. Y. Kwon et al., Quantum solvation and molecular rotations in superfluid helium clusters. J. Chem. Phys. **113**, 6469–6501 (2000). https://doi.org/10.1063/1.1310608
37. K. Szalewicz, Interplay between theory and experiment in investigations of molecules embedded in superfluid helium nanodroplets. Int. Rev. Phys. Chem. **27**, 273–316 (2008). https://doi.org/10.1080/01442350801933485
38. F. Dalfovo, Atomic and molecular impurities in ^{4}He clusters. Z. Phys. D Atom Mol. Cl. **29**, 61–66 (1994). https://doi.org/10.1007/BF01437166
39. F.R. Brühl et al., Rb-He exciplex formation on helium nanodroplets. J. Chem. Phys. **115**, 10220–10224 (2001). https://doi.org/10.1063/1.1410118
40. F. Stienkemeier et al., Spectroscopy of alkali atoms (Li, Na, K) attached to large helium clusters. Z. Phys. D Atom Mol. Cl. **38**, 253–263 (1996). https://doi.org/10.1007/s004600050090
41. F. Ancilotto et al., The binding of alkali atoms to the surfaces of liquid helium and hydrogen. Z. Phys. B Con. Mat. **98**, 323–329 (1995). https://doi.org/10.1007/BF01338398
42. F. Ancilotto et al., Physics of solvation. J. Low Temp. Phys. **101**, 1123–1146 (1995). https://doi.org/10.1007/Bf00754527
43. F. Ancilotto et al., Sodium dimers on the surface of liquid ^{4}He. Phys. Rev. B **52**, 16125–16129 (1995). https://doi.org/10.1103/PhysRevB.52.16125
44. A. Leal et al., Picosecond solvation dynamics of alkali cations in superfluid ^{4}He nanodroplets. Phys. Rev. B **90**, 224518 (2014). https://doi.org/10.1103/PhysRevB.90.224518
45. C. Stark, V.V. Kresin, Critical sizes for the submersion of alkali clusters into liquid helium. Phys. Rev. B **81**, 085401 (2010). https://doi.org/10.1103/PhysRevB.81.085401
46. L. An der Lan et al., The submersion of sodium clusters in helium nanodroplets: Identification of the surface → interior transition. J. Chem. Phys. **135**, 044309 (2011) https://doi.org/10.1063/1.3610388
47. L. An der Lan et al., Submersion of potassium clusters in helium nanodroplets. Phys. Rev. B **85**, 115414 (2012) https://doi.org/10.1103/PhysRevB.85.115414
48. Y. Ren, V.V. Kresin, Surface location of alkaline-earth-metal-atom impurities on helium nanodroplets. Phys. Rev. A **76**, 3 (2007). https://doi.org/10.1103/PhysRevA.76.043204
49. J.C. Hill et al., Evidence of Metastable Atomic and Molecular Bubble States in Electron-Bombarded Superfluid Liquid Helium. Phys. Rev. Lett. **26**, 1213–1216 (1971). https://doi.org/10.1103/PhysRevLett.26.1213
50. S.E. Huber, A. Mauracher, On the properties of charged and neutral, atomic and molecular helium species in helium nanodroplets: interpreting recent experiments. Mol. Phys. **112**, 794–804 (2014). https://doi.org/10.1080/00268976.2013.863403
51. H. Schöbel et al., High-resolution mass spectrometric study of pure helium droplets, and droplets doped with krypton. Eur. Phys. J. D **63**, 209–214 (2011). https://doi.org/10.1140/epjd/e2011-10619-1
52. L.F. Gomez et al., Sizes of large He droplets. J. Chem. Phys. **135**, 154201 (2011). https://doi.org/10.1063/1.3650235
53. C.B. Alcock et al., Vapour Pressure Equations for the Metallic Elements: 298–2500K. Can. Metall. Q. **23**, 309-313 (1984) DOI:
54. S. Ralser et al., Extracting cluster distributions from mass spectra: IsotopeFit. Int. J. Mass Spectrom. **379**, 194–199 (2015). https://doi.org/10.1016/j.ijms.2015.01.004
55. M. Renzler et al., On subthreshold ionization of helium droplets, ejection of He^+, and the role of anions. Phys. Chem. Chem. Phys. **16**, 22466–22470 (2014). https://doi.org/10.1039/c4cp03236e
56. A.A. Scheidemann et al., Capture of lithium by ^{4}He clusters: Surface adsorption, Penning ionization, and formation of $HeLi^+$. J. Chem. Phys. **107**, 2839–2844 (1997). https://doi.org/10.1063/1.474642
57. R. Dorrestein, Anregungsfunktionen metastabiler Zustände. In Helium und Neon, gemessen mit Hilfe der von metastabilen Atomen verursachten Elektronenauslösung aus Metallen. Physica **9**, 447-460 (1942) https://doi.org/10.1016/S0031-8914(42)90082-X
58. N. Halberstadt, K.C. Janda, The resonant charge hopping rate in positively charged helium clusters. Chem. Phys. Lett. **282**, 409–412 (1998). https://doi.org/10.1016/S0009-2614(97)01276-1
59. A.M. Ellis, S.F. Yang, Model for the charge-transfer probability in helium nanodroplets following electron-impact ionization. Phys. Rev. A **76**, 032714 (2007). https://doi.org/10.1103/PhysRevA.76.032714
60. B.E. Callicoatt et al., Charge transfer within He clusters. J. Chem. Phys. **105**, 7872–7875 (1996). https://doi.org/10.1063/1.472567
61. O. Echt et al., Magic Numbers for Sphere Packings: Experimental-Verification in Free Xenon Clusters. Phys. Rev. Lett. **47**, 1121–1124 (1981). https://doi.org/10.1103/PhysRevLett.47.1121
62. W.D. Knight et al., Electronic Shell Structure and Abundances of Sodium Clusters. Phys. Rev. Lett. **52**, 2141–2143 (1984). https://doi.org/10.1103/PhysRevLett.52.2141
63. P.W. Stephens, J.G. King, Experimental Investigation of Small Helium Clusters - Magic Numbers and the Onset of Condensation. Phys. Rev. Lett. **51**, 1538–1541 (1983). https://doi.org/10.1103/PhysRevLett.51.1538
64. P. Scheier, T.D. Märk, Metastable Decay of Singly Charged Argon Cluster Ions Ar_n^{+*}. Int. J. Mass Spectrom. Ion Processes **102**, 19–44 (1990). https://doi.org/10.1016/0168-1176(90)80050-D
65. R.G. Cooks et al., Chiroselective self-directed octamerization of serine: Implications for homochirogenesis. Anal. Chem. **73**, 3646–3655 (2001). https://doi.org/10.1021/ac010284l

66. M.Y. Chou et al., Total energies, abundances, and electronic shell structure of lithium, sodium, and potassium clusters. Solid State Commun. **52**, 645–648 (1984). https://doi.org/10.1016/0038-1098(84)90725-7
67. W.D. Knight et al., Electronic shell structure in potassium clusters. Solid State Commun. **53**, 445–446 (1985). https://doi.org/10.1016/0038-1098(85)91053-1
68. Y. Saito et al., Magic Numbers in a Mass Spectrum of Lithium Clusters Emitted from a Liquid Metal Ion-Source. Jpn. J. Appl. Phys. **27**, 424-427 (1988) https://doi.org/10.1143/jjap.27.424
69. N.D. Bhaskar et al., Evidence of electronic shell structure in Rb_N^+ (N=1-100) produced in a liquid-metal ion source. Phys. Rev. B **36**, 4418–4421 (1987). https://doi.org/10.1103/PhysRevB.36.4418
70. N.D. Bhaskar et al., Electronic-shell-structure effects in Cs_N^+. Phys. Rev. B **42**, 9147–9150 (1990). https://doi.org/10.1103/PhysRevB.42.9147
71. W.A. Deheer, The Physics of Simple Metal-Clusters - Experimental Aspects and Simple-Models. Rev. Mod. Phys. **65**, 611–676 (1993). https://doi.org/10.1103/RevModPhys.65.611
72. M. Lewerenz et al., Successive Capture and Coagulation of Atoms and Molecules to Small Clusters in Large Liquid-Helium Clusters. J. Chem. Phys. **102**, 8191–8207 (1995). https://doi.org/10.1063/1.469231
73. J. Harms et al., Density of superfluid helium droplets. Phys. Rev. B **58**, 3341–3350 (1998). https://doi.org/10.1103/PhysRevB.58.3341
74. Y.B. Li et al., Structure and dynamics of alkali-metal clusters and fission of highly charged clusters. Phys. Rev. B **57**, 15519–15532 (1998). https://doi.org/10.1103/PhysRevB.57.15519
75. M. Rosenblit, J. Jortner, Electron bubbles in helium clusters. I. Structure and energetics. J. Chem. Phys. **124**, 194505 (2006) https://doi.org/10.1063/1.2192780